International Journal of Offshore and Polar Engineering (ISSN 1053-5381)

Vol. 18, No. 4, December 2008, pp. 292–301

BEM Computations of 3-D Fully Nonlinear Free-Surface Flows Caused by Advancing Surface Disturbances

Hong Gun Sung*
Maritime & Ocean Engineering Research Institute (MOERI, formerly KRISO), Daejeon, Korea

Stéphan T. Grilli*
Department of Ocean Engineering, University of Rhode Island, Narragansett, Rhode Island, USA

We report on recent developments and validations of a numerical model for free-surface waves generated by an advancing surface disturbance. The model is based on potential flow theory with fully nonlinear free-surface boundary conditions. Equations are solved numerically in the time domain, using a 3-dimensional higher-order Boundary Element Method (HOBEM) combined with a 2nd-order explicit time updating. The generic model, developed in earlier work by Grilli et al. (2000, 2001), is extended in the paper to apply to the present forward-moving disturbance problem. We first assess both the accuracy and convergence rate of the HOBEM for a typical mixed Dirichlet-Neumann problem corresponding to the boundary value problem, which is solved at every time step in the computations. As expected, the convergence rate is found to be 3rd order, and mass and energy are conserved within less than 1% for highly nonlinear waves when at least 8 third-order boundary elements are used per wavelength. To achieve sufficient numerical efficiency for large and finely discretized problems, we use the Fast Multipole Algorithm (*N* log *N* method) recently tested in the model by Fochesato and Dias (2006). As a validation application, we compute 3-D nonlinear free-surface waves caused by a moving pressure patch, such as created by a Surface Effect Ship. Results show that the present methodology works quite well for numerical examples and gives reasonable wave resistance as compared with theory, and other computational results.

INTRODUCTION

According to linear wave theory, a disturbance advancing at steady speed on or below the free surface creates a so-called Kelvin wave pattern, which is completely described in the classical literature. However, surface waves created by a disturbance moving at high speed, such as a Surface Effect Ship (SES), and the resulting wave resistance, may significantly differ from this theory due to nonlinearity. In such cases, it is necessary to tackle the problem numerically and use nonlinear free-surface conditions. In this paper, we briefly review the state-of-the-art in computational methods for ship wave resistance and make recommendations for new directions of development, in light of our recent experience with 3-dimensional Boundary Element Method (BEM) computations of nonlinear free-surface flows (e.g. Grilli et al., 2000, 2001, 2008).

Wave resistance computations for a ship moving at constant forward speed have usually been formulated as a steady flow problem, in a reference frame moving with the ship. Such computations also yield sinkage and trim, which are 2 significant parameters for determining ship hull power requirements and operating condition (Sclavounos et al., 1997).

Initial work on waves generated by a moving vessel can be traced back to Wehausen, and many other precursors of naval hydrodynamics. Most of this classical work covers fundamental aspects and theoretical predictions of wave resistance for simple bodies, such as ship hulls with simplified analytic lines (Wehausen, 1973). A recent review of analytical representations of ship waves can be found in Noblesse (2000). When it comes to numerical computations of wave resistance, the BEM (initially referred to as "panel method" in its lowest approximation) has been widely used since the pioneering works of Hess and Smith (1964) and Dawson (1977). Thus, by the late 1970s, zero and non-zero forward speed problems were beginning to be solved with a BEM, in a so-called Neumann-Kelvin (NK) formulation in which the body boundary condition is satisfied on the mean position of the exact body surface, with linearized free-surface boundary conditions. A further refinement was to use the exact hull boundary condition, but still with linearized free-surface boundary conditions. This approach did not gain popularity, however, and Dawson (1977) devised the so-called double-body or Dawson's approach by linearizing about the double-body flow. An improvement along this line is the weak-scatter hypothesis of Pawloski (1991), where the wave disturbance caused by the ship motion is linearized around the ambient waves, while using the exact ship hull boundary condition; Huang and Sclavounos (1998) utilized this approximation for developing their SWAN 4 model.

By contrast, although more computationally demanding, the Fully Nonlinear Potential Flow (FNPF) approach does not require any approximation of the body or the free-surface boundary conditions. Jensen et al. (1989), Raven (1998), and Liu et al. (2001) reported initial results of using this approach for the steady forward motion. For the unsteady ship wave problem, a time-marching scheme must be used which, as indicated by Beck and Reed (2001), gives rise to additional difficulties, particularly when using an Eulerian-Lagrangian representation. Among these, a very important problem is the local treatment of breaking waves generated around the ship bow and stern, particularly for high-speed ships. Specifically, to be able to pursue numerical simulations with an FNPF-BEM beyond wave breaking, local absorption of wave energy in those regions of the free surface with nearly breaking

*ISOPE Member.

Received September 5, 2007; revised manuscript received by the editors May 20, 2008. The original version was submitted directly to the Journal.

KEY WORDS: Nonlinear free-surface flows, advancing disturbance, BEM (Boundary Element Method), higher-order BEM (HOBEM), accuracy and convergence, nonlinear pressure patch problem.

waves must be implemented. In this respect, Beck reported some success (1999) and, more recently, using a spilling breaker model, so have Muscari and Di Mascio (2004).

The main goal of this work is the application of an existing 3-D FNPF-BEM model (Grilli et al., 2000, 2001, 2008; Fochesato et al., 2005) to wave resistance computations for high-speed SES, such as the Harley FastShip, a new type of SES with catamaran hulls (e.g. Harris and Grilli, 2007). Initial results in this respect have been proposed by Sung and Grilli (2005, 2006).

In this paper we first present the mathematical and numerical formulations of the model, with an emphasis on the free-surface updating method. Next, we give simple applications, in which we assess the accuracy and rate of convergence of the HOBEM. Finally, we solve and validate the proposed methodology for the problem of nonlinear waves caused by a traveling pressure patch representing the air cushions of an SES.

GOVERNING EQUATIONS AND BOUNDARY CONDITIONS

We assume the fluid to be incompressible and inviscid, and the flow to be irrotational. We thus define the velocity potential, as the scalar function, $\Phi(\vec{x}, t)$, of spatial variables, $\vec{x} = (x, y, z) = (x_1, x_2, x_3)$, and time variable, t. The velocity potential is related to the fluid velocity vector, $\vec{u} = (u, v, w)$, by $\vec{u} = \nabla\Phi$, where ∇ denotes the gradient operator. With these definitions, mass conservation becomes Laplace's equation for the potential in the fluid domain, $\Omega(t)$:

$$\nabla^2\Phi(\vec{x}, t) = 0 \tag{1}$$

The boundary of the fluid domain is composed of a free surface, a body/ship boundary and external/far-field boundaries (lateral, downstream and upstream—Fig. 1). Appropriate boundary conditions (i.e., Dirichlet or Neumann) must be specified on the entire domain boundary.

In an Eulerian-Lagrangian representation, the kinematic and dynamic free-surface conditions are expressed as:

$$\frac{D\vec{R}}{Dt} = \vec{u} \equiv \nabla\Phi \tag{2}$$

$$\frac{D\Phi}{Dt} = -gz + \frac{1}{2}|\nabla\Phi|^2 - \frac{p_a}{\rho} \tag{3}$$

respectively, with $\vec{R} = (X, Y, Z)$ the free-surface position vector; g, the gravitational constant; ρ, the constant fluid density; p_a, the atmospheric or applied pressure on the free surface (e.g. due to the SES air cushions); and $D/Dt = \partial/\partial t + \vec{u}\cdot\nabla$, the material derivative.

For an Eulerian representation, we instead classically obtain:

$$\frac{\partial\zeta}{\partial t} = -\nabla_H\Phi\cdot\nabla_H\zeta + \frac{\partial\Phi}{\partial z} \tag{4}$$

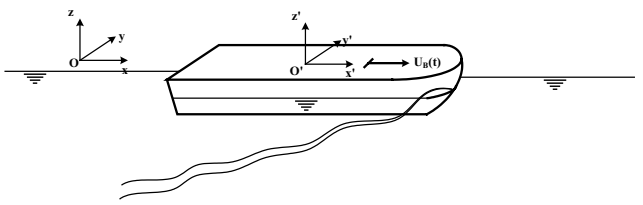

Fig. 1 Sketch of domain for unsteady forward speed problem ($U_B(t)$)

$$\frac{\partial\Phi}{\partial t} = -gz - \frac{1}{2}|\nabla\Phi|^2 - \frac{p_a}{\rho} \tag{5}$$

where ∇_H denotes the horizontal gradient operator (i.e. in the x and y directions). Below we detail the numerical time updating of the free-surface boundary conditions and geometry.

Under potential flow theory, the body boundary condition specifies that the normal velocity is continuous from the fluid to the body:

$$\nabla\Phi\cdot\vec{n} = \vec{V}\cdot\vec{n} \tag{6}$$

where $\vec{n} = (n_x, n_y, n_z)$ is the outwards unit normal vector, and $\vec{V}$ is the body velocity, either given by the specified motion of the disturbance (i.e. $\vec{V} = U_B\vec{e}_x$ for a forward speed problem) or obtained from the body equations of motion.

On the domain bottom and other fixed parts of the boundary (e.g. lateral boundary), a no-flow boundary condition is prescribed as:

$$\nabla\Phi\cdot\vec{n} = 0 \tag{7}$$

Far-field conditions are specified on the upstream and downstream boundaries. For instance, for a steady ship translation or an advancing pressure patch in still water, one can specify these as:

$$\lim_{r\to\infty}\nabla\Phi = (0, 0, 0) \tag{8}$$

where r denotes the radial distance from the source of the disturbance. Due to the domain finite length, the exact far-field condition (Eq. 8) will be modified, as detailed later in the paper. It is noted that all of the above equations were stated in a fixed coordinate system.

Free-Surface Time Updating Methods

The Lagrangian approach of free-surface time updating, based on Eqs. 2 and 3, which is also referred to as the material node approach, is more often used in problems with zero forward speed. An Eulerian description based on Eqs. 4 and 5 has also been used, particularly for nonlinear wave simulations in which wave overturning does not occur. The advantages of the former method are that its formulation is very straightforward, and that it provides fluid particle trajectories under wave motion. One of the difficult numerical issues with the Lagrangian method is that fluid markers tend to accumulate around stagnation points and regions of relatively high flow speed, which may cause numerical instability (e.g. Beck, 1999; Grilli et al., 2001). One can circumvent this difficulty in time-marching schemes by relocating (or regridding) fluid markers from time to time (Grilli et al., 2001). Although straightforward in principle, regridding poses some practical difficulties. By contrast, regridding is not required with the Eulerian method, but one has to numerically evaluate the horizontal gradient of the free-surface elevation, to be used in Eq. 4, and the method is limited to single-valued free-surface elevation.

For forward speed problems, such as the present case of wave generation by an advancing disturbance (Fig. 1), the Eulerian method has advantages over the Lagrangian method, which when expressed in earth-fixed coordinates usually requires a longer computational domain in order to reach steady state. Further, grid resolution must be very dense around the disturbance (or ship) to capture the steeper waves generated around the bow and stern. Hence, such calculations may be time-consuming and inefficient for very large, finely discretized, computational domains. A practical solution to this problem is to use a coordinate system moving

with the disturbance and adopt an Eulerian or pseudo-Lagrangian updating.

For forward speed problems in a moving reference frame, the total velocity potential is expressed as the sum of the free-stream velocity potential, which corresponds to the translation of the disturbance, and the perturbed potential. Beck (1999) solved this problem with a pseudo-Lagrangian updating, which allows surface markers to follow a prescribed path. To do so, he defined a time derivative following the moving nodes as $\delta/\delta t = \partial/\partial t + \vec{v}\cdot\nabla$, where $\vec{v}$ is the velocity of a moving node (which may be different from that of the actual fluid particles). It is noted that this approach can be regarded as an Eulerian updating method. Similarly to this conventional approach, Sung and Grilli (2005) proposed a new scheme of free-surface time updating, in which fictitious fluid particles keep the values of their x-coordinates stationary in the moving reference frame. Accordingly, the free-surface boundary conditions read:

$$\frac{\tilde{D}\vec{R}}{\tilde{D}t'} = W_y\vec{e}_y + W_z\vec{e}_z \tag{9}$$

$$\frac{\tilde{D}\Phi}{\tilde{D}t'} = \Phi_{t'} + W_y\frac{\partial\Phi}{\partial y} + W_z\frac{\partial\Phi}{\partial z} \tag{10}$$

where primes denote variables in the moving reference frame, $\vec{e}_y$ and $\vec{e}_z$ are the unit vectors in the y- and z-directions, and $\vec{W} = (W_x, W_y, W_z)$ is the pseudo-Lagrangian velocity defined as:

$$W_x = U_B(t),\ W_y = \frac{\partial\Phi}{\partial y},\ W_z = \frac{\partial\Phi}{\partial z} - \frac{n^x}{n^z}\left[U_B(t) - \frac{\partial\Phi}{\partial x}\right] \tag{11}$$

Summarizing the above, 3 different approaches of free-surface time updating were used in past applications: the material node (the Lagrangian); the Eulerian; and the pseudo-Lagrangian. We present below yet a new method of time updating that proves more relevant and efficient when applied to our problem than any of the earlier methods.

Combined Method of Free-Surface Time Updating

To draw maximum benefit from the time updating methods detailed above, we now combine the Lagrangian and Eulerian (or pseudo-Lagrangian) methods as follows:

- We express boundary conditions in the conventional moving reference frame, where we also solve the boundary integral equation using a higher-order 3-D BEM.
- The Eulerian wave elevation, $\zeta^E(x, y, t)$ is obtained from Eqs. 9 and 10, assuming waves do not overturn at the next time step.
- The Lagrangian wave elevation, $\zeta^L(x, y, t)$, is obtained from Eqs. 2 and 3, after correcting fluid marker velocities (see below), because the coordinate system is moving with the free-surface disturbance speed.
- The 2 free-surface profiles are linearly combined using a user-defined interpolation function, $\gamma(x, y, t)$, e.g. defined as:

$$\zeta = [1 - \gamma(x, y, t)]\zeta^E + \gamma(x, y, t)\zeta^L$$

$$\gamma(x, y, t) = \begin{cases} 1 & (x, y) \in S^L \\ \gamma \in (0, 1) & (x, y) \in S^T \\ 0 & (x, y) \in S^E \end{cases} \tag{12}$$

where S^L denotes the free-surface region in which the Lagrangian representation is used, S^E the remaining Eulerian region, and S^T a transition region from S^L to S^E, with gradual variation of one time updating method to the other. Given the problem definition for an advancing disturbance and the particular grid system selected, one can usually specify an appropriate shape for the 3 regions (S^L, S^T and S^E) for which the numerical solution will converge.

According to Eqs. 12, the surface elevation function ζ must be single-valued in both the transition and Eulerian regions but can become multiple-valued in the Lagrangian region (although this will usually terminate computations when the touch down of a plunging jet occurs on the free surface). However, a wave-absorption algorithm can be easily applied in the Lagrangian zone to prevent wave overturning, e.g. based on the absorbing pressure algorithm detailed in Grilli and Horrillo (1997). This is detailed below.

Finally, note that in this method the Eulerian (outer) region can also be replaced by a pseudo-Lagrangian zone S^P, such as was done in the work of Sung and Grilli (2005).

SOLUTION METHODOLOGY

HOBEM

The governing Eq. 1, with time-dependent nonlinear free-surface boundary conditions Eqs. 2 and 3, is solved using the higher-order 3-D FNPF-BEM model of Grilli et al. (2000, 2001) with extensions detailed in Fochesato et al. (2005). These references should be consulted for details of the numerical implementation. The model is modified to apply to the moving disturbance problem.

The main aspects of the higher-order BEM are summarized below. Green's second identity transforms Eq. 1 into the following BIE:

$$\alpha(\vec{x}_l)\Phi(\vec{x}_l) = \int_\Gamma \left[\frac{\partial\Phi}{\partial n}(\vec{x})G(\vec{x}, \vec{x}_l) - \Phi(\vec{x})\frac{\partial G}{\partial n}(\vec{x}, \vec{x}_l)\right] d\Gamma \tag{13}$$

where $\alpha(\vec{x}_l)$ is the normalized interior solid angle at point $\vec{x}_l$; $G(\vec{x}, \vec{x}_l) = 1/4\pi r$ is the free-space Green's function, where $r = |\vec{r}| = |\vec{x} - \vec{x}_l|$ is the distance from the source point $\vec{x}$ to the field point $\vec{x}_l$ (both on the boundary); $\partial G/\partial n(\vec{x}, \vec{x}_l) = -\vec{r}\cdot\vec{n}/4\pi r^3$; and $\vec{n}$ is the outward unit vector normal to the boundary at point $\vec{x}$.

Eq. 13 is discretized and solved by a BEM, using bi-cubic piecewise overlapping boundary elements, based on the Mid-Interval-Interpolation method (MII). In such elements, the local interpolation of both the boundary geometry and variables is expressed in 4×4 node sliding elements, of which only one quadrilateral (usually the central one) is used in the integrations. A curvilinear transformation is applied to express equations onto a single reference element. The numerical integration for source and doublet influence coefficients is as follows:

Regular integrals are calculated by a bi-directional Gauss-Legendre quadrature method.

Weakly singular integrals, in which distance r vanishes, are handled by first applying a polar coordinate transformation to regularize the integral kernel, and then Gauss-Legendre numerical integration.

Quasi-singular integrals, in which distance r becomes very small but non-zero, are computed by using a so-called adaptive integration scheme, in which successive subdivisions of the element are made based on distance and solid angle criteria.

Time Integration

As detailed in Grilli et al. (2001), 2nd-order truncated Taylor series expansion are used to update both the position vector $\vec{R}$ and the velocity potential Φ on the free surface. The resulting time-marching scheme for the free-surface evolution, for instance, reads:

$$\vec{R}(\breve{t}_n+\delta\breve{t}_n)=\vec{R}(\breve{t}_n)+\frac{\breve{D}\vec{R}}{\breve{D}\breve{t}}\delta\breve{t}_n+\frac{\breve{D}}{\breve{D}\breve{t}}\left[\frac{\breve{D}\vec{R}}{\breve{D}\breve{t}}\right]\frac{(\delta\breve{t}_n)^2}{2} \tag{14}$$

where the form of $\breve{D}/\breve{D}\breve{t}$ varies depending upon the type of method used for free-surface updating, as discussed above.

Higher-order Spatial Derivatives

One can show that 2nd-order Lagrangian and pseudo-Lagrangian time derivatives in Eqs. 2 and 3, or Eqs. 9 and 10, respectively, can be expressed as a function of 1st- and 2nd-order time and spatial derivatives of the potential. The normal derivatives are obtained as solution of the BEM equations. The tangential derivatives are calculated based on the boundary solution, in a 5×5 quartic sliding element, as detailed in Grilli et al. (2001). It is noted that Fochesato et al. (2005) developed improved formulations of tangential derivatives in the model, which are used in the present applications.

Solution to Linear Algebraic Equations

The linear system of algebraic BEM equations is solved using the iterative solver GMRES (Generalized Minimal RESidual), combined with the FMA (Fast Multipole Algorithm), an efficient N log N method implemented by Fochesato and Dias (2006) in the 3-D BEM model and applied to tsunami and freak wave generation and propagation by Enet and Grilli (2005) and Fochesato et al. (2007), respectively. (See also Grilli et al., 2008.) The relationship of computational time to discretization size N is studied below, in the context of present applications.

NUMERICAL RESULTS

Accuracy and Convergence of Computations

As mentioned earlier, Grilli et al. (2000, 2001) originally developed the core of the BEM model and numerical algorithms. Aspects of model efficiency, convergence and accuracy were initially analyzed in these papers for 3-D wave propagation, shoaling and breaking, using a direct matrix solver. Later, Guyenne and Grilli (2006) used the iterative solver GMRES and reported improved performance on a vector computer. Fochesato and Dias (2006) implemented the FMA in the model and similarly tested model performance, finding the expected N log N convergence rate of computations. In the following, we perform a similar analysis of numerical errors as a function of discretization size, in the context of the present implementation of the model. To do so, we solve a simple but representative case of linear periodic wave propagation in a rectangular domain, for which there is an exact solution in the form:

$$\begin{aligned}&\Phi=\frac{gA_I}{\omega}\frac{\cosh k(z+h)}{\cosh kh}\sin\Theta\\&\Theta=k_x x+k_y y-\omega t+\theta;\ k=\sqrt{k_x^2+k_y^2};\ \omega^2=gk\tanh kh\end{aligned} \tag{15}$$

where A_I denotes the wave amplitude, k the wave number (k_x and k_y are the wave numbers along each direction), ω the circular frequency, and θ the phase function. The last equation in Eq. 15 is the linear dispersion relationship, relating the wave number to the frequency, in depth h. The computation domain shown in Fig. 2 is a rectangular region similar to that used in later applications. The velocity potential is specified as a boundary condition on the free surface, and its normal derivative Φ_n is specified on the other boundaries, both based on Eq. 15.

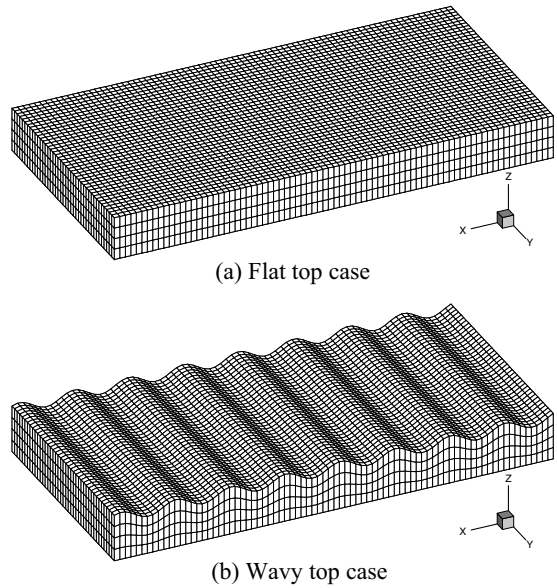

(a) Flat top case

(b) Wavy top case

Fig. 2 Domain and grid systems used for accuracy and convergence studies based on linear wave theory (vertical scale magnified)

In all calculations, the domain length, l_x is 8 times the wavelength λ and depth is set to unity. The number of elements ranges from 4 to 16 per wavelength in the x direction, and the element length along y is set equal to that along x. The number of elements on the vertical sides is kept constant to 4.

Numerical errors are defined as the absolute difference between the analytic and numerical solutions, normalized by dividing by the maximum value of the associated variable on the corresponding boundary. Errors are calculated for the potential normal gradient on the Dirichlet boundary, S_D, which corresponds to the free surface, and for the potential on the Neumann boundary, S_N, which includes the other boundaries. In each case, we calculate the maximum error, $\varepsilon^{\max}$, mean error, $\varepsilon^{\text{mean}}$, and rms (root mean square) error, ε^{rms}. Thus, for example, $\varepsilon_D^{\max}$, $\varepsilon_D^{\text{mean}}$ and $\varepsilon_D^{\text{rms}}$ are the maximum, mean and rms errors on the Dirichlet boundary.

Fig. 3 shows numerical errors calculated on the Dirichlet boundary as a function of the element size δx, normalized by the wavelength, for a rectangular domain with a flat free surface.

Power curve fits of errors shown in Fig. 3 as function of relative mesh size yield:

$$\varepsilon_D^{\max}\approx 20.64(\delta x/\lambda)^{3.57} \tag{16}$$

$$\varepsilon_D^{\text{mean}}\approx 4.62(\delta x/\lambda)^{3.48} \tag{17}$$

$$\varepsilon_D^{\text{rms}}\approx 6.85(\delta x/\lambda)^{3.61} \tag{18}$$

which indicates a rate of convergence of the solution close to a power 3.5. This could have been expected considering the cubic interpolation functions used in the BEM elements. Additionally, we see for instance that approximately 6 elements per wavelength must be used to achieve a 1% mean error level on the Dirichlet boundary.

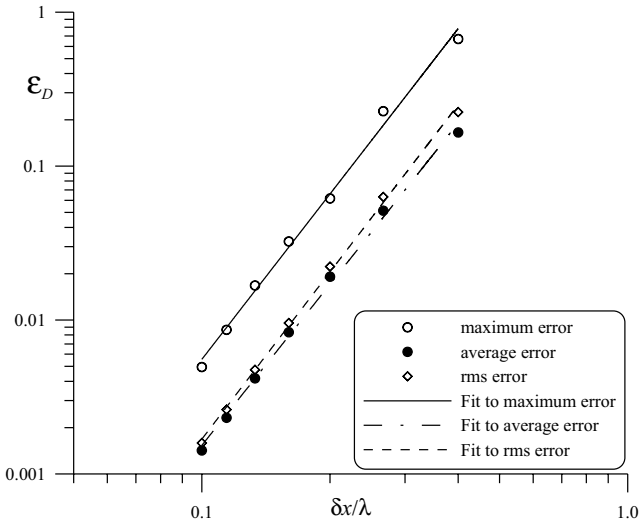

Fig. 3 Numerical errors on Dirichlet boundary as function of normalized element size (rectangular domain with flat top)

Fig. 4 shows numerical errors for the Neumann boundary, which are found to be smaller, by almost one order of magnitude, than errors on the Dirichlet boundary. This is a known feature of the BEM solution for mixed Dirichlet-Neumann problems, having been already identified and discussed by Grilli et al. (2001) in the context of this 3-D BEM model, and for another BEM model by Sung (1999). Additionally, power curve fits indicate that error convergence rates are slightly better than for the Dirichlet boundary.

$$\varepsilon_N^{\max} \approx 12.32(\delta x/\lambda)^{4.04} \tag{19}$$

Fig. 5 shows that, in the above computations, computational time grows like the power 1.3 of the number of unknowns:

$$\text{CPU Time(secs)} \approx 0.0016N^{1.32} \tag{20}$$

This is close to the expected optimal growth of computational time with the number of unknowns for the FMA.

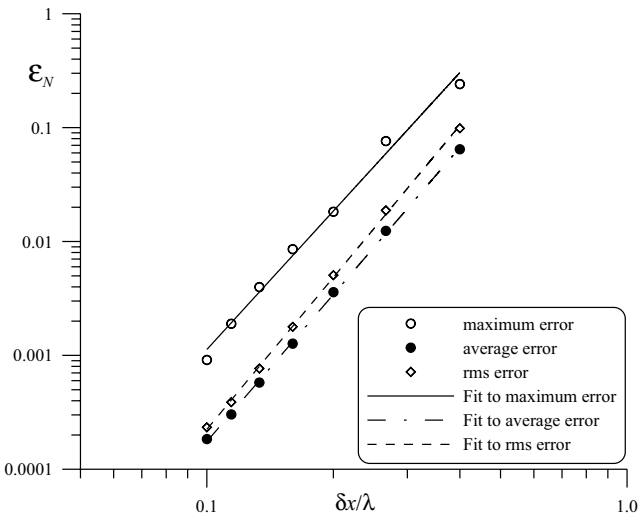

Fig. 4 Numerical errors on Neumann boundary as function of normalized element size (rectangular domain with flat top)

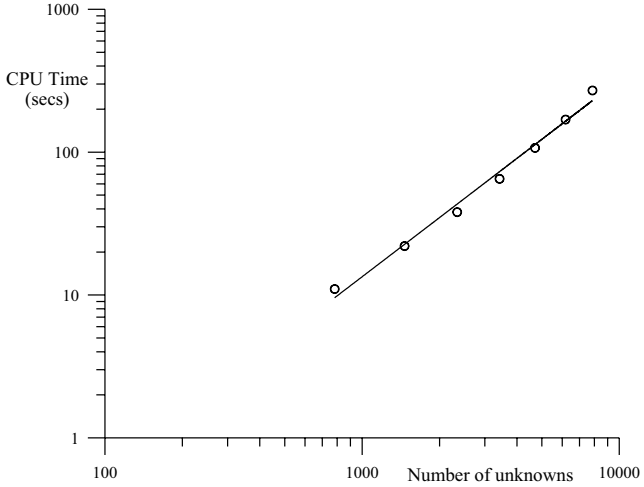

Fig. 5 Computational time of present method for case of Figs. 1∼3 (rectangular domain with flat top)

The accurate computation of flow velocities on the free surface is of great importance for the global accuracy of the numerical method, when applied to nonlinear time-domain simulations of surface waves. Free-surface velocity and acceleration are indeed used to update the fluid domain geometry and potential at every time step. Fig. 6 shows numerical errors for flow velocities computed on the free surface as a function of discretization size. Curve fits to the results show that errors on the velocity ε_V behave approximately as follows:

$$\varepsilon_V^{\max} \approx 73.58(\delta x/\lambda)^{3.34} \tag{21}$$

$$\varepsilon_V^{\text{mean}} \approx 8.16(\delta x/\lambda)^{3.47} \tag{22}$$

$$\varepsilon_V^{\text{rms}} \approx 14.45(\delta x/\lambda)^{3.57} \tag{23}$$

hence similarly to other errors on the Dirichlet boundary. This was expected since these errors combine normal velocities, which are directly provided by the BEM solution, and tangential velocities, which are calculated by interpolation of the exact potential.

Next we examine the effect of a wavy rather than flat free surface on the numerical solution by using the analytic extension

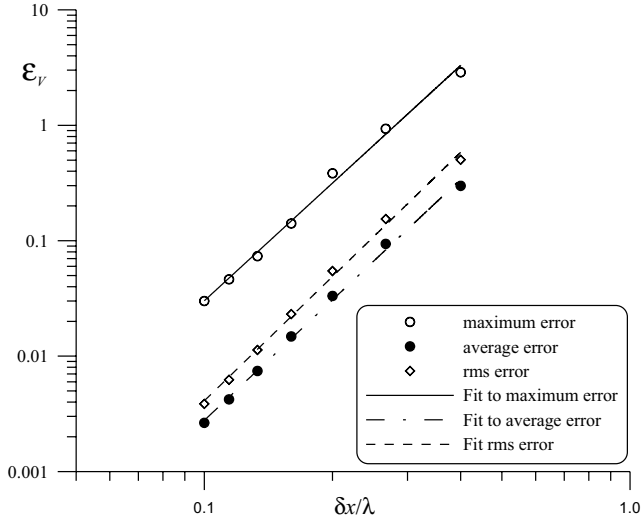

Fig. 6 Numerical errors of module of flow velocity on free surface (rectangular domain with flat top)

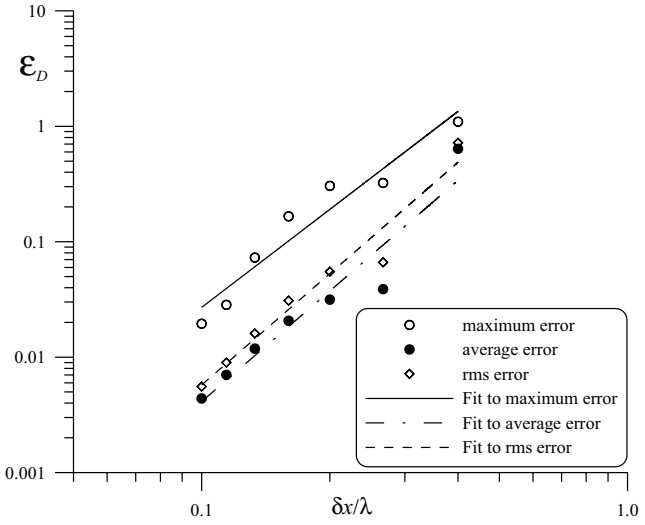

Fig. 7 Numerical errors on Dirichlet boundary as function of normalized element size (rectangular domain with wavy top)

of the velocity potential up to the exact wave elevation (rather than the mean water level). This is possible because the analytic functions defining the potential are not restricted to the lower half space. The analytical free surface is obtained by applying the linearized free-surface condition to the potential in Eq. 15 as:

$$\zeta(x, y, t) = A_I \cos\Theta \tag{24}$$

Fig. 2b shows the grid system for these computations. The boundary value problem, constructed in the same manner as for the flat free surface, now more closely corresponds to the boundary value problem solved at every time step in time-domain computation of nonlinear free-surface waves. Fig. 7 shows numerical errors on the Dirichlet boundary for this case, for $A_I/\lambda = 1/10$, which corresponds to a strongly nonlinear case. Both the accuracy and rate of convergence are somewhat reduced as compared to the flat top case in Fig. 3. Through curve fitting, we find:

$$\varepsilon_D^{\max} \approx 11.87(\delta x/\lambda)^{2.82} \tag{25}$$

$$\varepsilon_N^{\max} \approx 49.13(\delta x/\lambda)^{4.63} \tag{26}$$

Thus we can conclude that, for the case of a wavy free surface, the convergence of the present model solution is nearly 3rd order with respect to the element size. When the coarsest case is excluded in the accuracy estimates, we find that for highly nonlinear waves it is necessary to use a minimum of 8 elements per wavelength to achieve numerical errors smaller than 1%. Hence, for a wavy free surface we must use a slightly more refined mesh to achieve the same level of accuracy as for a flat free surface. By contrast, on the Neumann boundary, errors are slightly smaller for a wavy free surface than for a flat surface, but this could just be an artifact of the selected test case.

Waves Generated by Advancing Pressure Patch

In this first application of the full numerical model, we validate the proposed combined updating methodology by computing nonlinear waves, and the corresponding wave resistance, caused by a pressure patch specified on the free surface and accelerating from a state of rest to a steady state. This problem has been studied earlier using theoretical or numerical methods, in relation

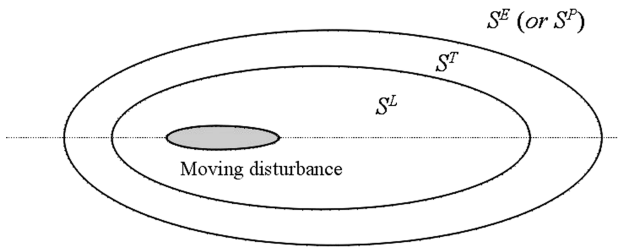

Fig. 8 Definition sketch of free-surface regions used in combined updating method: Lagrangian (S^L), Transition (S^T), Eulerian (S^E) or Pseudo-Lagrangian (S^P)

to the design of conventional Air Cushion Vehicles (ACV) (e.g. Doctors and Sharma, 1972; Wyatt, 2000; Sung and Grilli, 2005).

Before discussing numerical results, we further detail the main features of the 3 regions, with different free-surface time updating methods, used in computations: Lagrangian (S^L), Transition (S^T), and Eulerian (S^E) or Pseudo-Lagrangian (S^P) regions. Fig. 8 shows a sketch of the 3 zones, in which elliptical shapes have been used to delineate the boundary of each zone. (Note that, in principle, any arbitrary shape could be used depending upon the problem and areas of interest.) We solve 4 different test cases, referred to as C1-C4, which differ by the size of each region used for free-surface time updating (Table 1). Of the 4 cases, C4 has the largest S^L region and is thus defined as our reference case. Numerical results are first compared between cases and later with results obtained in earlier work.

As in Doctors and Sharma (1972), we define the theoretical shape of the pressure patch representing the moving disturbance as:

$$\begin{aligned} p_a = M(t)\frac{p_0}{4}&[\tanh\alpha(x' - x_0 + a) - \tanh\alpha(x' - x_0 - a)] \\ &\times [\tanh\beta(y - y_0 + b) - \tanh\beta(y - y_s 0 - b)] \end{aligned} \tag{27}$$

in which a time ramp-up function $M(t)$ is used for gradually starting simulations:

$$M(t) = \frac{1}{2}\left\{1 - \cos\frac{\pi t}{T_m}\right\} \tag{28}$$

for $t \le T_m$, and $M(t) = 1$ for later times $t > T_m$.

Numerical results are normalized by setting $2a = 1.0$, $g = 1.0$ and $\rho = 1.0$. Hence the characteristic quantities for length, time, velocity, velocity potential and pressure variables are L, $\sqrt{g/L}$, $\sqrt{gL}$, $L\sqrt{gL}$ and ρgL, respectively, where L is a characteristic length. In the following, we use symbol ($\wedge$) to denote normalized quantities. We also use a cosine ramp-up function for the translation velocity of the pressure patch.

Case Number Dimensions	C1	C2	C3	C4
Length of major axis of S^L	2.0	3.0	4.5	6.5
Length of minor axis of S^L	1.0	2.0	3.0	3.0
Length of major axis of S^T	2.5	5.0	7.5	9.5
Length of minor axis of S^T	1.5	3.0	4.5	4.5
Coordinates of center	(8,0)	(8,0)	(8,0)	(10,0)

Table 1 Parameters of elliptical free-surface regions used in combined updating method

Wave resistance due to the motion of the disturbance is obtained as the pressure force on the disturbed free surface within the cushion:

$$R_w = -\int_{S_{AC}} pn_x dS \tag{29}$$

where S_{AC} denotes the air-cushion surface area. This physical quantity is made dimensionless as $R_c = (R_w/W)(\rho g a/p_0)$, where $W = 4\rho g a p$ is the weight supported by the pressure patch.

In the coordinate system traveling at the instantaneous velocity of the moving disturbance, no-flow boundary conditions are applied on the downstream, upstream and sidewall boundaries of the domain, which thus move at the same speed as the pressure patch. An absorbing pressure is specified over a narrow strip of the free surface next to the upstream boundary in order to prevent the growth of small sawtooth instabilities that could be created due to the amplification of small numerical errors by the relative fluid flow velocity (Sung and Grilli, 2005). Grid point clustering is prevented on the free surface by regridding nodes at every time step in the simulations.

Unless otherwise noted, we use the following parameter values: $L = 2a$, $\hat{p}_0 = 0.025$, $b/a = 0.5$, $\alpha a = \beta a = 5$ and $\hat{U}_B^{\max} = -1$ (dimensionless advancing velocity of the pressure patch). The computational domain is 18 dimensionless units long and 10 wide, and there are 81 and 15 node points in the x and y directions, respectively, yielding an initial grid size of about 0.22 unit in each direction. The water depth is $\hat{d} = 1$ (finite depth case). Throughout the simulations, the time step and normalized modulation time are kept constant at $\delta\hat{t} = 0.05$ and $\hat{T}_m = 2.0$.

Fig. 9 shows time histories of the relative difference between wave resistance computed as a function of time for cases C1-C3 and the reference case C4. Results are normalized by the steady-state value of wave resistance for C4. We see that results converge to those of C4, which is the most accurate solution in the full Lagrangian zone, as the area of the Lagrangian zone (S^L) is increased. Considering the very small differences with C4, case C3 could probably be used as well as the reference solution.

Fig. 10 shows the time evolution of free-surface waves around the traveling pressure patch for C4. Fig. 11 compares the wave resistance coefficient R_c computed with (*i*) full Lagrangian, (*ii*) pseudo-Lagrangian, and (*iii*) the present combined updating method (the latter with zones of Case C4). In each case, nonlinear time-domain simulations are performed in the computation domain of the same size, with the same grid system. The agreement is quite good after quasi-steady state is reached at

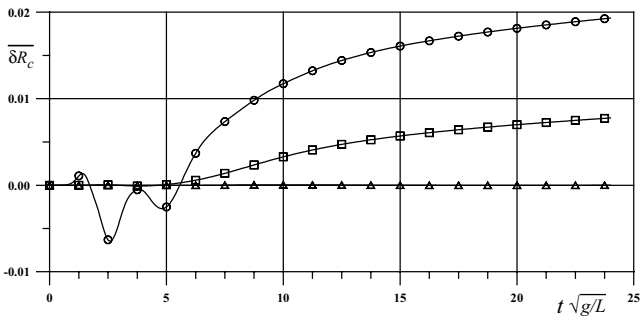

Fig. 9 Effect of size of time-updating regions (Table 1) on total wave resistance—relative difference with C4 plotted by normalizing with steady-state value of R_c for C4: (○) = C1, (□) = C2, (△) = C3

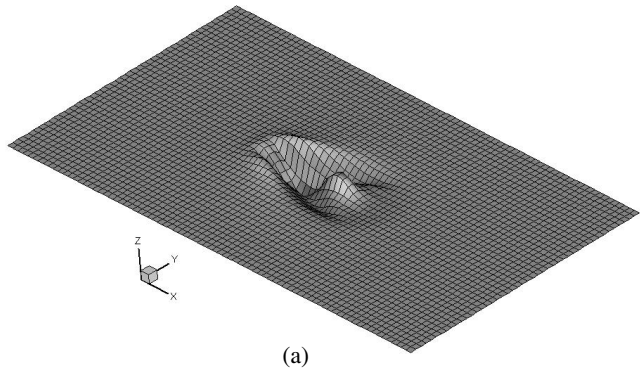

(a)

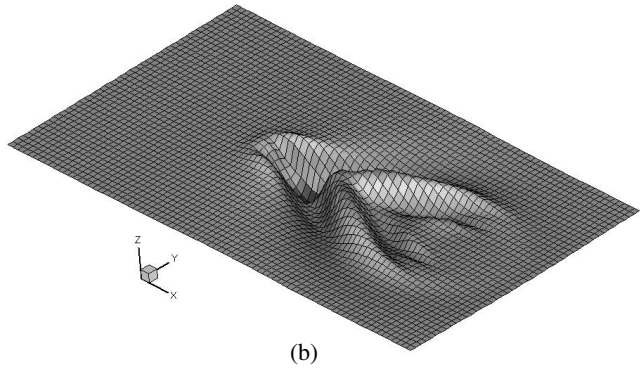

(b)

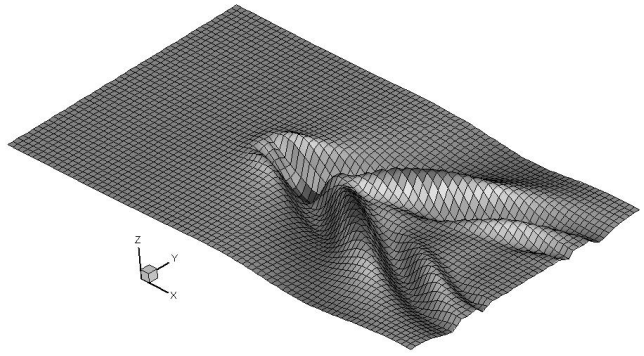

(c)

Fig. 10 Free-surface evolution of advancing pressure patch problem computed using combined time updating method, with zones of case C4 (Table 1), at $\hat{t} =$ (a) 4, (b) 8, (c) 12

$\hat{t} = 12 \sim 13$. The predicted values of the steady-state wave resistance are:

- 0.971 (full-Lagrangian updating)
- 0.970 (pseudo-Lagrangian updating)
- 0.986 (the present combined method)

For the sake of comparison, linear wave theory yields 1.041 (Doctors and Sharma, 1972). In the Lagrangian updating, because a fixed domain is used, the pressure patch eventually reaches the fixed upstream boundary, which terminates computations; also, the downstream vertical surface causes reflection and fluctuations in the computed wave resistance at larger times. The pseudo-Lagrangian method is that reported in earlier results by Sung and Grilli (2005). It can then be concluded that the present numerical approach, with a new combined free-surface updating methodology, provides accurate and efficient results (in the sense that a much shorter domain can be used than with the full Lagrangian method, while retaining the advantages of the Lagrangian updating near the moving disturbance).

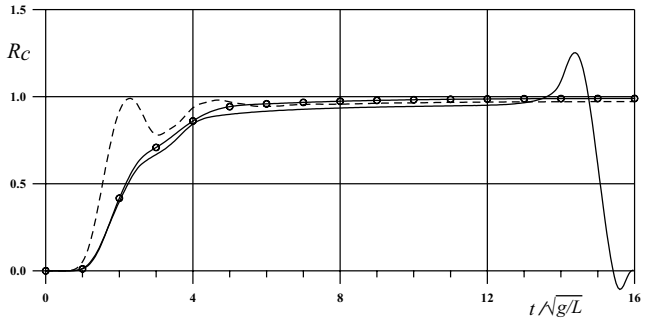

Fig. 11 Time history of wave resistance coefficient for traveling pressure patch with updating method = solid line; full Lagrangian = dashed line; pseudo-Lagrangian, and circles = combined method with zones of Case C4

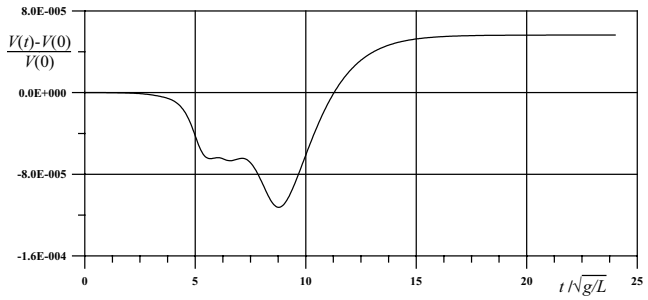

Fig. 12 Mass conservation of computational domain for traveling pressure patch with present combined update and zones of case C4

In order to check the global accuracy of the combined method, we compute time histories of total volume, kinetic, potential and total energy for the case in Fig. 10. After computations have reached the steady state, the maximum relative error on the total volume of the computational domain is less than 0.006% (Fig. 12). Fig. 13 shows that the total energy becomes constant after reaching steady state, with a nearly equal partition of kinetic and potential energy.

Fig. 14 shows the steady-state free-surface wave patterns obtained using the 3 different updating methods discussed above. As expected, significant reflection occurs at the downstream boundary for the full Lagrangian method, and fluctuations can also be seen at the upstream free-surface boundary. These fluctuations do not occur in the pseudo-Lagrangian and the present updating methods. It is also noted that, with the full Lagrangian updating method, an

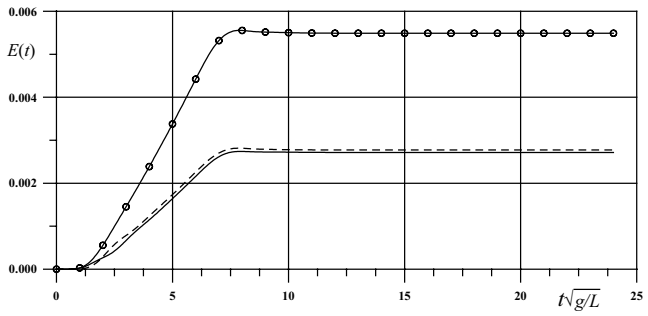

Fig. 13 Wave energy for traveling pressure patch, with present combined updating method and zones of case C4 (same case as in Fig. 10): solid = kinetic energy ($K.E.$); dashed = potential energy ($P.E.$); and circles = total energy ($T.E. = P.E. + K.E.$)

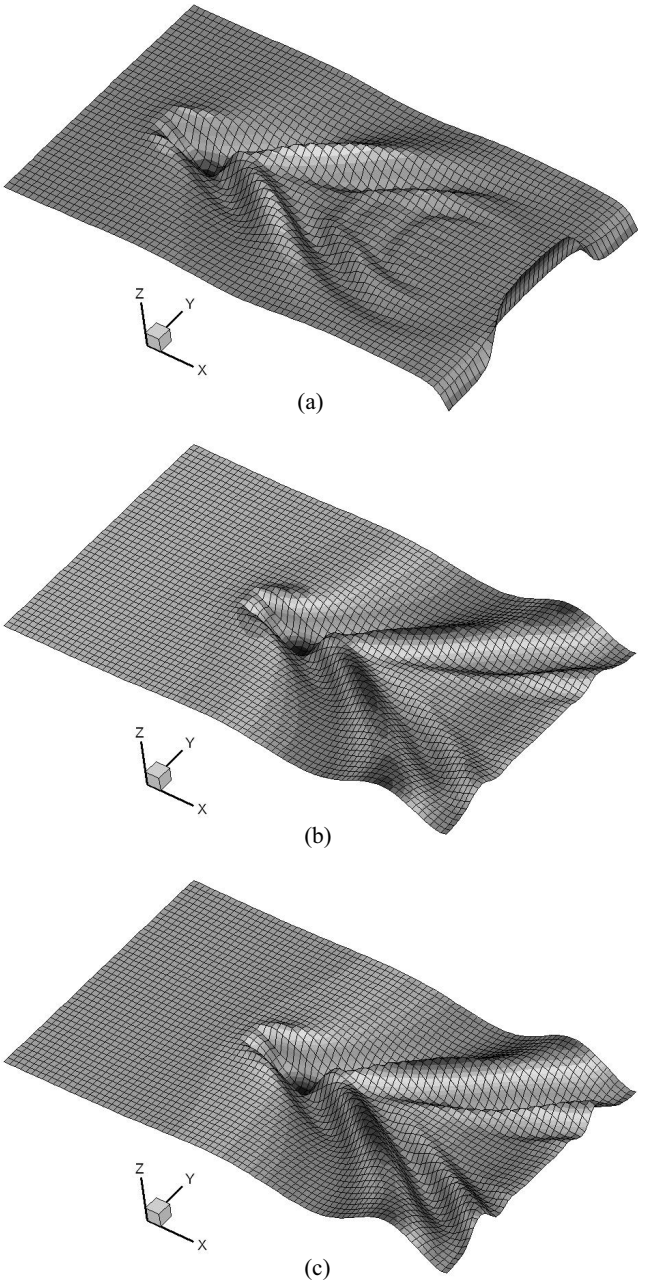

Fig. 14 Comparison of steady-state free-surface profiles (same case as in Fig. 10) for updating method: (a) full Lagrangian, (b) pseudo-Lagrangian, (c) combined (zones of case C4)

open boundary condition was specified on the downstream boundary of the earth-fixed computation domain, as a pressure sensitive "snake absorbing piston wave-maker" (Brandini and Grilli, 2001; Fochesato et al., 2007).

Fig. 15 shows the wave resistance coefficient computed as a function of the pressure patch velocity, using the combined method with zones of Case 4. The faster the pressure patch, the earlier the wave resistance coefficient reaches steady state, and the smaller it is.

The steady-state values of wave resistance coefficients in Fig. 15 are compared in Fig. 16 with those obtained by other free-surface updating methods or predicted by linear wave theory (Doctors and Sharma, 1972). We see that all of the nonlinear methods yield smaller wave resistance results than the linear method for the selected case. Further, the present combined

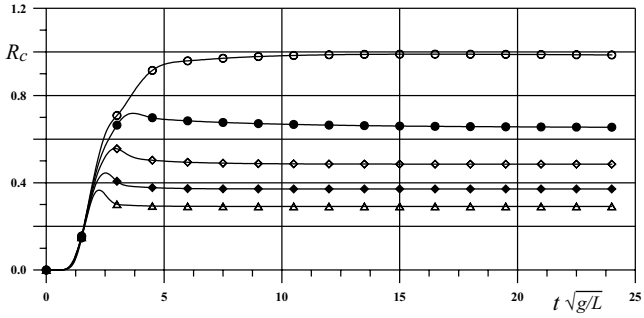

Fig. 15 Wave resistance coefficient as function of pressure patch velocity, using combined updating method and zones of case C4: (○) $\hat{U}_B^{\max} = -1.00$, (●) $\hat{U}_B^{\max} = -1.25$, (◇) $\hat{U}_B^{\max} = -1.50$, (◆) $\hat{U}_B^{\max} = -1.75$, and (△) $\hat{U}_B^{\max} = -2.00$

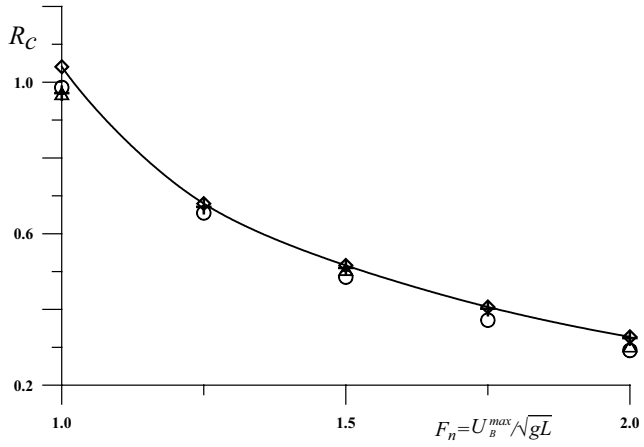

Fig. 16 Wave resistance coefficient computed with: (○) combined updating method with zones of case C4, (△) full Lagrangian updating, (+) pseudo-Lagrangian updating (Sung and Grilli, 2005), and (—) linear wave theory (Doctors and Sharma, 1972)

method of free-surface updating gives slightly smaller values of wave resistance than other free-surface updating methods.

CONCLUSIONS

Using the 3-D higher-order BEM model (HOBEM) originally developed by Grilli et al. (2000, 2001), with recent extensions by Fochesato et al. (2005) and Fochesato and Dias (2006), we developed a new combined methodology for simulating nonlinear free-surface flows generated by an advancing surface disturbance. As expected from the 3rd-order accurate spatial and temporal discretizations, in the BEM model, result convergence is of 3rd order as a function of the grid size, and numerical errors of less than 1% for highly nonlinear waves can be achieved when using at least 8 elements per wavelength. Using the Fast Multipole Algorithm (FMA) in the BEM solver, we confirmed that CPU time almost linearly increases with the number of unknowns. In conclusion, when properly discretized, the present BEM model yields both an accurate and converged efficient solution when modeling 3-D nonlinear water waves in the context of a mixed Dirichlet-Neumann problem, such as the wave resistance problem in a traveling system of axes.

Numerical results obtained for waves generated by a traveling pressure patch show that the new proposed method, for identical accuracy, is more efficient than the conventional full Lagrangian and pseudo-Lagrangian methods, such as used earlier by Sung and Grilli (2005).

Further work must be done for modeling nonlinear waves generated by an advancing surface-piercing body, but in principle, the model should achieve a similar performance for such problems. Such work will be presented in a future paper completing the present study.

ACKNOWLEDGEMENTS

The authors acknowledge support from a grant from Ocean Dynamics Inc., Wickford, Rhode Island, USA, awarded to the University of Rhode Island. The first author's work was partially supported by the Post-doctoral Fellowship Program of the Korea Science & Engineering Foundation (KOSEF), and by the principal R&D program of KORDI: Development of Extreme Response Analysis Technologies for Offshore Structures granted by the Korea Research Council of Fundamental Science and Technology.

REFERENCES

Beck, RF (1999). "Fully Monlinear Water Wave Computations Using a Desingularized Euler-Lagrange Time Domain Approach," *Nonlinear Water Wave Interaction*, O Mahrenholtz and M Markiewicz, eds, Adv in Fluid Mech Series, WIT Press, pp 1–58.

Beck, RF, and Reed, AM (2001). "Modern Computational Methods for Ships in a Seaway," *SNAME Trans*, Vol 109, pp 1–51.

Brandini, C, and Grilli, ST (2001), "Modeling of Freak Wave Generation in a 3D-NWT," *Proc 11th Offshore and Polar Eng Conf*, Stavanger, ISOPE, Vol 3, pp 124–131.

Dawson, CW (1977). "A Practical Computer Method for Solving Ship-wave Problems," *Proc 2nd Int Conf Num Ship Hydrodyn*, Berkeley, CA, pp 30–38.

Doctors, LJ, and Sharma, SD (1972). "The Wave Resistance of an Air-Cushion Vehicle in Steady and Accelerated Motion," *J Ship Res*, Vol 16, pp 248–260.

Enet, F, and Grilli, ST (2005). "Tsunami Landslide Generation: Modelling and Experiments," *Proc 5th Int Ocean Wave Measurement and Analysis*, Madrid, IAHR Pub, Paper 88.

Fochesato, C, and Dias, F (2006). "A Fast Method for Nonlinear 3-D Free-Surface waves," *Proc Royal Soc A*, pp 2715–2735.

Fochesato, C, Grilli, ST, and Dias, F (2007). "Numerical Modeling of Extreme Rogue Waves Generated by Directional Energy Focusing," *Wave Motion*, Vol 44, pp 395–416.

Fochesato, C, Grilli, ST, and Guyenne, P (2005). "Note on Nonorthogonality of Local Curvilinear Coordinates in a 3-D Boundary Element Method," *Int J Num Meth in Fluids*, Vol 48, pp 305–324.

Grilli, ST, Dias, F, Guyenne, P, Fochesato, C, and Enet, F (2008). "Progress In Fully Nonlinear Potential Flow Modeling of 3-D Extreme Ocean Waves," *Advances in Numerical Simulation of Nonlinear Water Waves* (Series in Adv in Coastal and Ocean Eng), World Sci Pub, 55 pp (in press).

Grilli, ST, Guyenne, P, and Dias, F (2000). "Modeling of Overturning Waves over Arbitrary Bottom in 3-D Numerical Wave Tank," *Proc 10th Int Offshore and Polar Eng Conf*, Seattle, ISOPE, Vol 3, pp 221–228.

Grilli, ST, Guyenne, P, and Dias, F (2001). "A Fully Nonlinear Model for 3-D Overturning Waves over an Arbitrary Bottom," *Int J Num Meth in Fluids*, Vol 35, pp 829–867.

Grilli, ST, and Horrillo, J (1997). "Numerical Generation and Absorption of Fully Nonlinear Periodic Waves," *J Eng Mech*, Vol 123, pp 1060–1069.

Guyenne, P, and Grilli, ST (2006). "Numerical Study of 3-D Overturning Waves in Shallow Water," *J Fluid Mech*, Vol 547, pp 361–388.

Harris, JC, and Grilli, ST (2007). "Computation of the Wavemaking Resistance of a Harley Surface Effect Ship," *Proc 17th Offshore and Polar Eng Conf*, Lisbon, ISOPE, Vol 3, pp 732–739.

Hess, JL, and Smith, AMO (1964). "Calculation of Nonlinear Potential Flow About Arbitrary 3-D Bodies," *J Ship Res*, Vol 8, No 2, pp 22–44.

Huang, Y, and Sclavounos, PD (1998). "Nonlinear Ship Motions," *J Ship Res*, Vol 42, No 2, pp 120–130.

Jensen, G, Bertram, V, and Söding, H (1989). "Ship Wave-resistance Computations," *Proc 5th Int Conf Num Ship Hydrodyn*, Hiroshima, pp 593–606.

Liu, Y, Xue, M, and Yue, DKP (2001). "Computations of Fully Nonlinear 3-D Wave-Wave and Wave-Body Interactions—Part 2: Nonlinear Waves and Forces on a Body," *J Fluid Mech*, Vol 438, pp 41–66.

Muscari, R, and Di Mascio, A (2004). "Numerical Modeling of Breaking Waves Generated by a Ship's Hull," *J Marine Sci and Tech,* Vol 9, pp 158–170.

Noblesse, F (2000). "Analytical Representation of Ship Waves," *23rd Weinblum Memorial Lecture*, Hydrodynamic Directorate Tech Rept NSWCCD-TR-2000/011, NSWC, Carderock Div.

Pawloski, JS (1991). "A Theoretical and Numerical Model of Ship Motions in Heavy Seas," *SNAME Trans*, Vol 99, pp 319–352.

Raven, HC (1998). "Inviscid Calculations of Ship Wave Making—Capabilities, Limitations, and Prospects," *Proc 22nd Symp Ship Hydrodyn*, Washington, DC, pp 738–754.

Saad, Y, and Schultz, MH (1986). GMRES: A Generalized Minimal Residual Algorithm for Solving Nonsymmetric Linear Systems, SIAM, *J Sci Statistic Comp*, No 7, pp. 856–869.

Sclavounos, PD, Kring, DC, Huang, Y, Mantzaris, DA, Kim, S, and Kim, Y (1997). "A Computational Method as an Advanced Tool of Ship Hydrodynamic Design," *SNAME Trans*, Vol 5, pp 375–397.

Sung, HG (1999). "A Numerical Analysis of Nonlinear Diffraction Problem in 3 Dimensions by Using Higher-order Boundary Element Method," *PhD Thesis*, Seoul National Univ.

Sung, HG, and Grilli, ST (2005). "Numerical Modeling of Nonlinear Surface Waves Caused by Surface Effect Ship: Dynamics and Kinematics," *Proc 15th Offshore and Polar Eng Conf*, ISOPE, Seoul, Vol 3, pp 124–131.

Sung, HG, and Grilli, ST (2006). "Combined Eulerian-Lagrangian or Pseudo-Lagrangian Descriptions of Waves Caused by an Advancing Free-Surface Disturbance," *Proc 16th Offshore and Polar Eng Conf*, San Francisco, ISOPE, Vol 3, pp 487–494.

Sung, HG, Hong, Sa Y, and Choi, Hang S (2000). "Evaluation of Nonlinear Wave Forces on a Fixed Body by Higher-order Boundary Element Method," *J Mech Eng Sci* (*Proc Inst Mech Eng, Part C*), Vol 214, pp 825–839.

Wehausen, JV (1973). "The Wave Resistance of Ships," *Adv in Appl Mech*, Vol 13, pp 93–245.

Wyatt, DC (2000). "Development and Assessment of a Nonlinear Wave Prediction Methodology for Surface Vessels," *J Ship Res*, Vol 44, No 2, pp 96–107.